Detection and Analysis of Clear-Sky, Low-Level Atmospheric Temperature Inversions with MODIS

YINGHUI LIU

Cooperative Institute for Meteorological Satellite Studies, University of Wisconsin—Madison, Madison, Wisconsin

JEFFREY R. KEY

NOAA/NESDIS/Office of Research and Applications, Madison, Wisconsin

(Manuscript received 20 November 2002, in final form 27 May 2003)

ABSTRACT

The near-surface atmosphere of the polar region is characterized by temperature inversions throughout most of the year. However, radiosonde data are sparse, and numerical weather prediction models have relatively poor vertical resolution for boundary layer studies. A method is developed for detecting and estimating the characteristics of clear-sky, low-level temperature inversions using the Moderate Resolution Imaging Spectroradiometer (MODIS) on the *Terra* and *Aqua* satellites. The method is based on an empirical relationship between the inversion strength, defined as the temperature difference across the inversion, or depth, defined as the altitude difference, and the difference between brightness temperatures in the 7.2-μm water vapor and 11-μm infrared window bands. Results indicate that inversion strength can be estimated unbiasedly with a root-mean-square error (rmse) of 2°–3°C and an R^2 of 0.80–0.97. Inversion depth can be estimated with an rmse of 130–250 m and an R^2 of 0.62–0.82. With MODIS, temperature inversions can be observed at a spatial resolution as high as 1 km^2 and a temporal sampling of up to 14 times per day, providing an opportunity for detailed studies of the spatial distribution and temporal evolution of the high-latitude boundary layer.

1. Introduction

Low-level atmospheric temperature inversions are ubiquitous at high latitudes during the low-sun and dark periods of the year. Temperature differences across inversions range from a few degrees to more than 30°C, depending on the season and altitude, and their heights are commonly lower than 700 hPa. Inversions are associated with stably stratified, persistent conditions that decouple the surface from the lower troposphere above the inversion. They influence the magnitude of heat and moisture fluxes through openings in the sea ice, the depth of vertical mixing in the boundary layer, cloud formation, aerosol transport, surface wind velocity, and lead formation.

Temperature inversions in the polar region may result from radiative cooling, warm air advection over a cooler surface layer, subsidence, and topography. Kahl (1990) examined the climatological characteristics of low-level tropospheric temperature inversions based on radiosonde data from two coastal weather stations. Serreze et al. (1992) investigated the seasonal and regional variations in characteristics of the Arctic low-level temperature inversion using radiosonde data from Arctic inland and coastal sites and Soviet drifting stations. Bradley et al. (1992) examined the annual cycle of surface-based inversions at nine Arctic weather stations based on radiosonde data. Bradley et al. (1993) and Walden et al. (1996) analyzed the systematic change in midwinter surface-based inversion depth over the past few decades based on the radiosonde data from several weather stations in the Arctic. Stone and Kahl (1991) examined Antarctic temperature inversions. All of these studies used radiosonde data to characterize the temporal distributions of inversions.

Unfortunately, meteorological stations that provide radiosonde data are sparsely distributed across the Arctic and Antarctic, and therefore provide little information on the spatial distribution of temperature inversions. Can satellite data be used to observe temperature inversion structure? There are operational atmospheric sounders on polar-orbiting satellites that provide reasonably accurate temperature profiles overall, but retrieval methods are not optimized for the lower troposphere. In this paper we extend the work of Ackerman (1996), who found that large negative brightness temperature differences between infrared window and water vapor channels of the High Resolution Infrared Sounder (HIRS) over Antarctica were associated with atmo-

Corresponding author address: Yinghui Liu, CIMSS, University of Wisconsin—Madison, 1225 West Dayton St., Madison, WI 53706. E-mail: yinghuil@ssec.wisc.edu

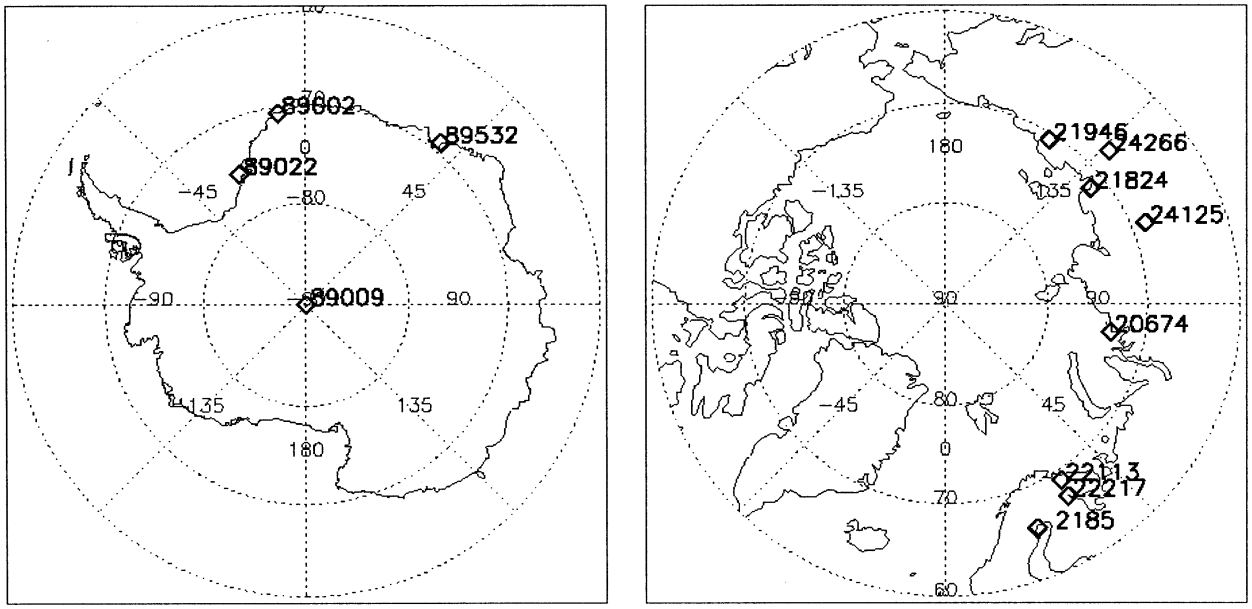

FIG. 1. Locations of the (left) Antarctic and (right) Arctic weather stations used in this study. Additional details are provided in Table 1.

spheric temperature inversions. Here we use spectral bands that measure water vapor and carbon dioxide closer to the surface than the 6.7-μm band used by Ackerman (1996) and are therefore able to detect weaker and shallower inversions. Empirical equations for estimating the inversion strength, defined as the temperature difference between the surface and the top of the inversion, and depth, defined as the altitude of the maximum inversion temperature above the surface, are presented. The methods are then applied to a sample of Moderate Resolution Imaging Spectroradiometer (MODIS) scenes in both polar regions, and the estimated inversion characteristics are compared to those from a numerical model and from another retrieval method. Results are restricted to clear-sky conditions because thermal satellite sensors cannot measure surface or near-surface conditions under cloud cover.

TABLE 1. Meteorological stations used in this study.

Station ID (WMO no.)	Lat N:+ S:−	Lon E:+ W:−	Station elevation (m)	Station
89002	−70.67	−8.25	40	Neumayer
89009	−90.0	0.0	2830	Amundsen-Scott
89022	−75.5	−26.65	30	Halley
89532	−69.0	39.58	21	Syowa
02185	65.55	22.13	16	Lulea/Kallax
20674	73.53	80.40	47	Ostrov Dikson
21824	71.58	128.92	8	Tiksi
21946	70.62	147.90	61	Cokurdah
22113	68.97	33.05	51	Murmansk
22217	67.15	32.35	26	Kandalaksa
24125	68.50	112.43	220	Olenek
24266	67.55	133.38	137	Verhojansk

2. Data

The soundings data used in this study are from four Antarctic and eight Arctic meteorological stations (Fig. 1) for the period October 2000 to March 2002. Table 1 gives the name, location, and elevation of each station. The atmospheric sounding data for the South Pole were obtained from the Antarctic Meteorological Research Center at the University of Wisconsin—Madison. The data are high-resolution, with measurements taken at intervals of approximately 3 s. The standard-resolution data for the other stations were obtained from the National Oceanic and Atmospheric Administration (NOAA) Forecast System Laboratory. The radiosonde data are twice daily at 0000 and 1200 UTC. Pressure, height, temperature, and dewpoint temperature are available for each sounding. While more radiosonde stations exist, only those stations listed in Table 1 provide data that can be matched with satellite overpasses.

Of the 12 stations, the South Pole has a very high surface elevation at 2830 m above mean sea level; the others have surface elevations less than 250 m. As will be demonstrated below, surface elevation plays an important role in the development of the temperature inversion retrieval methods. Therefore, all data are separated into two groups: the high-surface-elevation data from the South Pole and the low-surface-elevation data from the other 11 weather stations. Due to the thermal lag of thermistors used on radiosondes, temperatures measured by an instrument rising at a few meters per second can be biased. Mahesh et al. (1997) recommends a thermal lag correction for all situations in which radiosondes are used to measure steep temperature gra-

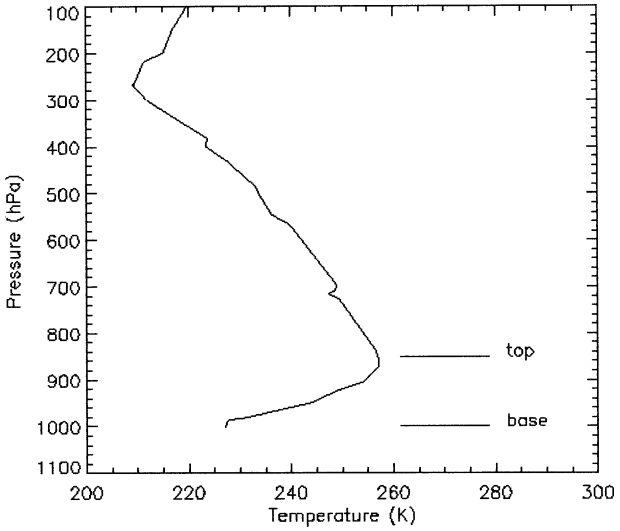

FIG. 2. Temperature profile measured at Verhojansk, Russia, 1200 UTC 3 Dec 2001. Temperature inversion top and base are indicated.

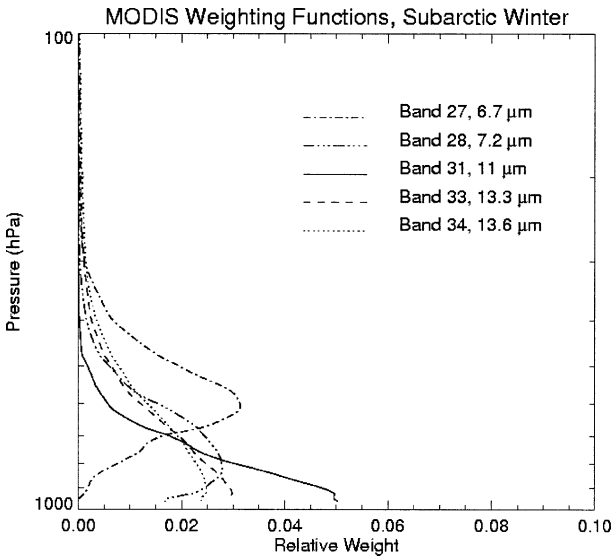

FIG. 3. Weighting functions for the MODIS bands at 6.7, 7.2, 11, 13.3, and 13.6 μm using subarctic winter standard atmosphere profile.

dients in the boundary layer. The correction method was applied to the radiosonde data used in this study.

The MODIS on board the National Aeronautics and Space Administration (NASA) *Terra* and *Aqua* polar-orbiting satellites provides global observations of the earth's land, oceans, and atmosphere in the visible and infrared regions of the spectrum at 36 wavelengths from 0.4 to 14.5 μm. The MODIS data product used in this study, called ''MOD07_L2'' (King et al. 2003), has a 5-km spatial resolution and provides brightness temperatures for 12 infrared channels (numbers 24–36, 4.5–14.3 μm), retrieved temperature profiles at 20 pressure levels under clear conditions, and a cloud mask. The MODIS data were obtained from the NASA Goddard Space Flight Center Distributed Active Archive Center (DAAC).

Only clear-sky cases are examined, as determined by the cloud mask in the MOD07_L2 dataset. For each clear-sky radiosonde profile, the closest MODIS 5-km pixel in time and space is used. In all there are 165 collocated radiosonde–MODIS samples for the high-surface-elevation group and 255 collocated samples for the low-surface-elevation group. The samples cover all seasons.

Temperature profiles from the National Centers for Environmental Prediction–National Center for Atmospheric Research (NCEP–NCAR) reanalysis project are used for comparison with MODIS retrievals, obtained from NOAA's Climate Diagnostics Center. The data provide air temperature and geopotential height at 17 pressure levels (1000, 925, 850, 700, 600, 500, 400, 300, 250, 200, 150, 100, 70, 50, 30, 20, 10 hPa) 4 times per day at 0000, 0600, 1200, and 1800 UTC. The spatial resolution of the data is 2.5° latitude $\times$ 2.5° longitude.

3. Theoretical basis

In this study we are concerned only with clear-sky temperature inversions in the lower troposphere. Inversions are assumed to have their bases at the surface, so the base height is the meteorological station elevation. The top of the inversion is the height with the maximum temperature measurement in the radiosonde profile below 400 hPa. If the maximum temperature is within an isothermal layer, the top of the inversion is defined as the height at the top of the isothermal layer. The inversion strength is defined as the difference between the surface temperature and the temperature at the inversion top. The temperature inversion depth is defined as the altitude difference between the surface and the temperature inversion top. Figure 2 shows a typical temperature profile with a temperature inversion.

Upwelling thermal radiation measured by MODIS is a function of the atmospheric transmittance at a given wavelength and the atmospheric temperature. The channel weighting function, which is the derivative of transmittance with respect to pressure, describes the degree to which radiation emitted at various vertical levels contributes to the upwelling radiance. Figure 3 gives the relative weighting functions for MODIS channels 27 (6.7 μm), 28 (7.2 μm), 31 (11 μm), 33 (13.3 μm), and 34 (13.6 μm), calculated for the subarctic winter standard atmosphere. Channels 27 and 28 are water vapor channels, 31 is a window channel, and 33 and 34 are carbon dioxide channels. The peaks of the weighting functions for the 6.7-, 7.2-, 11-, 13.3-, and 13.6-μm channels are approximately 600 hPa, 800 hPa, the surface, 950 hPa, and 900 hPa, respectively. Because the weighting functions are broad and represent an average radiance contribution from a layer, the measured brightness temperature is sensitive to a relatively thick layer. The weighting functions will be somewhat different for different absorber amounts and atmospheric pressure, the latter being a function of surface elevation.

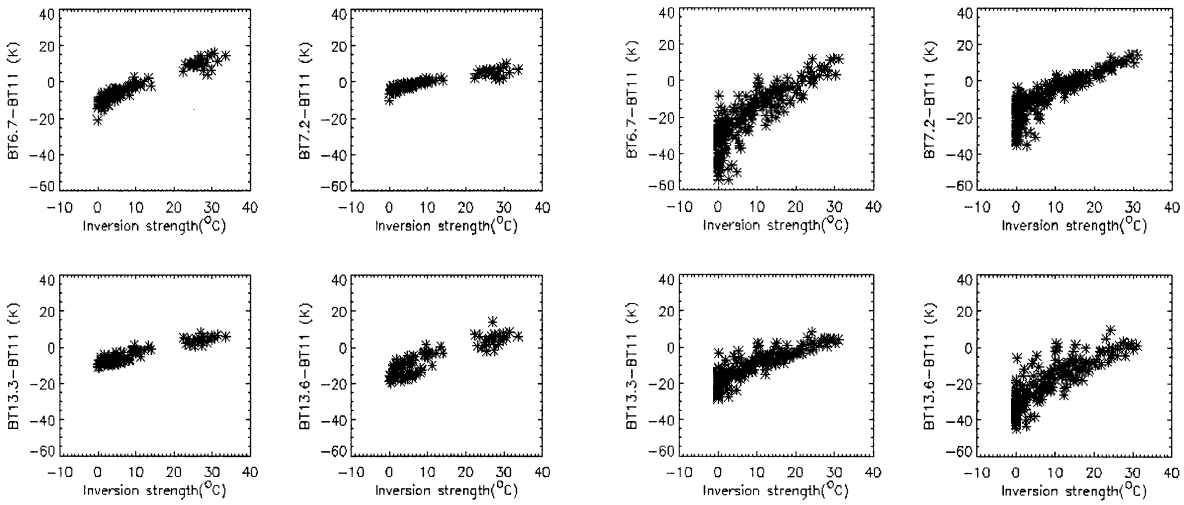

FIG. 4. Relationship between simulated brightness temperature difference pairs and the temperature inversion strength over (left) high-elevation surfaces and (right) low-elevation surfaces.

As Fig. 3 shows, the brightness temperature of the window channel at 11 μm, BT_{11}, will be most sensitive to the temperature of the surface. The 7.2-μm water vapor channel brightness temperature, $BT_{7.2}$, is most sensitive to temperatures near 800 hPa. The magnitude of the brightness temperature difference (BTD) between the 7.2- and 11-μm channels, $BT_{7.2} - BT_{11}$, will therefore be proportional to the strength of temperature difference between the 800-hPa layer and the surface, which is related to the inversion strength. This should also be true for the two 13-μm carbon dioxide channels. The 6.7-μm water vapor channel peaks near 600 hPa, so $BT_{6.7} - BT_{11}$ can also provide information about inversion strength. In the Arctic and the low-elevation areas of the Antarctic, the temperature inversion top is typically below 700 hPa (Serreze et al. 1992; Bradley et al. 1992), so $BT_{7.2} - BT_{11}$ will better represent the inversion strength than will $BT_{6.7} - BT_{11}$. Also, $BT_{7.2} - BT_{11}$ is more effective than $BT_{13.3} - BT_{11}$ and $BT_{13.6} - BT_{11}$ in providing information on inversion strength because the surface contribution is larger at 13.3 and 13.6 μm than at 7.2 μm. On the Antarctic plateau, where the surface pressure is typically 600–700 hPa, water vapor amount is low, and inversions are strong and deep, both $BT_{7.2} - BT_{11}$ and $BT_{6.7} - BT_{11}$ can provide useful information on inversion strength.

The brightness temperature difference is not only a function of the temperature inversion strength but also the inversion depth. To illuminate the relationship between BTDs and both inversion strength and inversion depth, the radiative transfer model Streamer (Key and Schweiger 1998) is used to simulate MODIS brightness temperatures. The model can simulate the brightness temperature at each MODIS infrared channel for each radiosonde temperature and humidity profile. Simulations and subsequent analyses with observations are done separately for low- and high-elevation surfaces. On average, inversion properties are different for low- and high-altitude locations because of the climatological ranges in surface temperature, atmospheric water vapor, and, of course, surface pressure. Therefore, weighting functions and the relationship between inversion characteristics and BTDs also differ.

Figure 4 shows the simulated relationship between different BTD pairs and the temperature inversion strength for high- and low-surface-elevation conditions. There are strong linear relationships for all channel pairs and both surface-elevation categories. Figure 5 shows the relationship between the simulated BTD pairs and the temperature inversion depth for high- and low-elevation surfaces. For high-elevation surfaces the relationships are weak, especially when the BTD is large. For low-elevation surfaces the linear relationships are stronger. For both elevation categories, larger BTDs indicate greater inversion depth.

Based on the relationships shown in Figs. 4 and 5 it appears that MODIS data can, in theory, be used to estimate inversion strength and inversion depth. Are similar relationships apparent in the MODIS data? Figure 6 shows the relationship between different BTDs and the temperature inversion strength for high- and low-surface-elevation conditions based on actual MODIS and collocated radiosonde data. For high-elevation conditions, the correlation coefficients between temperature inversion strength and $BT_{6.7} - BT_{11}$, $BT_{7.2} - BT_{11}$, $BT_{13.3} - BT_{11}$, and $BT_{13.6} - BT_{11}$ are 0.97, 0.98, 0.95, and 0.93, respectively. Figure 7 shows the relationship between MODIS BTDs and radiosonde-derived inversion depth. For high-elevation conditions, the correlation coefficients between temperature inversion depth and $BT_{6.7} - BT_{11}$, $BT_{7.2} - BT_{11}$, $BT_{13.3} - BT_{11}$, and $BT_{13.6} - BT_{11}$ are 0.89, 0.90, 0.88, and 0.87, respectively. The relationships are similar to those shown in Figs. 4 and 5.

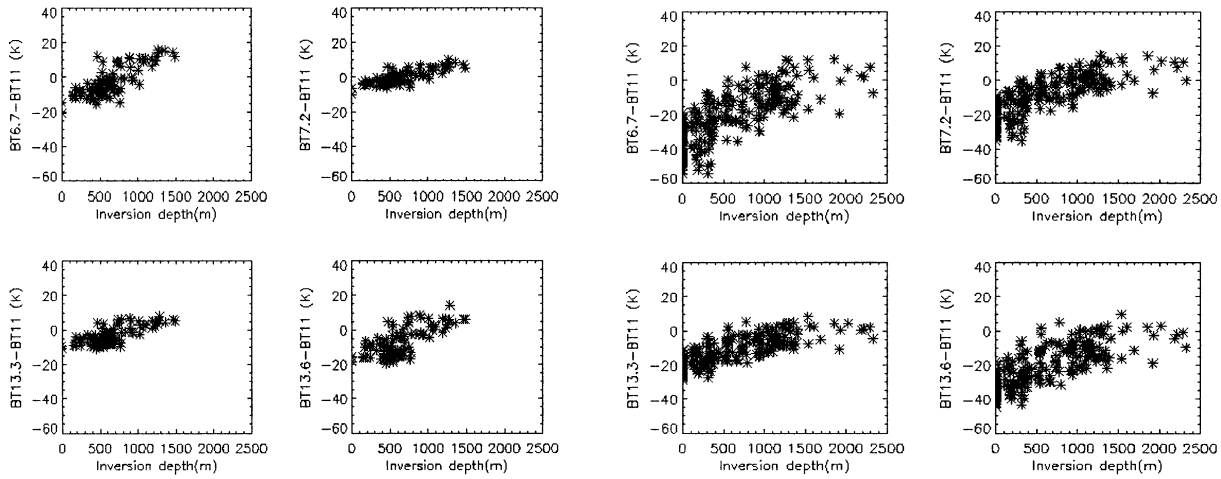

FIG. 5. Relationship between simulated brightness temperature difference pairs and the temperature inversion depth with (left) high-elevation surfaces and (right) low-elevation surfaces.

4. Retrieval of temperature inversion strength and depth

a. Temperature inversion detection

To estimate the inversion strength using MODIS infrared brightness temperature data under clear conditions, it is first necessary to determine if, in fact, an inversion is present. This step is separate from the retrieval of inversion characteristics because the relationship between BTD and inversion strength is poor for weak, shallow inversions (Figs. 4 and 6, right). We therefore choose to eliminate such inversions from the analysis. Since BTD increases with the increasing inversion strength, a threshold is chosen to identify those conditions without inversions or with weak inversions. There is no single threshold that can unambiguously identify inversions. In this study we use $BT_{6.7} - BT_{11}$ as the inversion detection test with a threshold of -20 K, such that a $BT_{6.7} - BT_{11}$ value greater than -20 K indicates the presence of an inversion. For high-surface-elevation areas like the interior of Antarctica, $BT_{6.7} - BT_{11}$ is always greater than -20 K, which indicates that temperature inversions are common throughout the year. In the Arctic and low-surface-elevation areas of the Antarctic, some (but not all) inversions with strengths between 0° and 10° will be missed. Overall, more than 70% of the inversions will be detected with this threshold. Unfortunately, about 7% of the noninversion cases will be misidentified as inversions.

b. Retrieval of temperature inversion strength

After applying the simple inversion threshold test and further excluding observed inversions with strengths less than 2 K that were not eliminated by the threshold test (collectively about 15% of the cases), the relation-

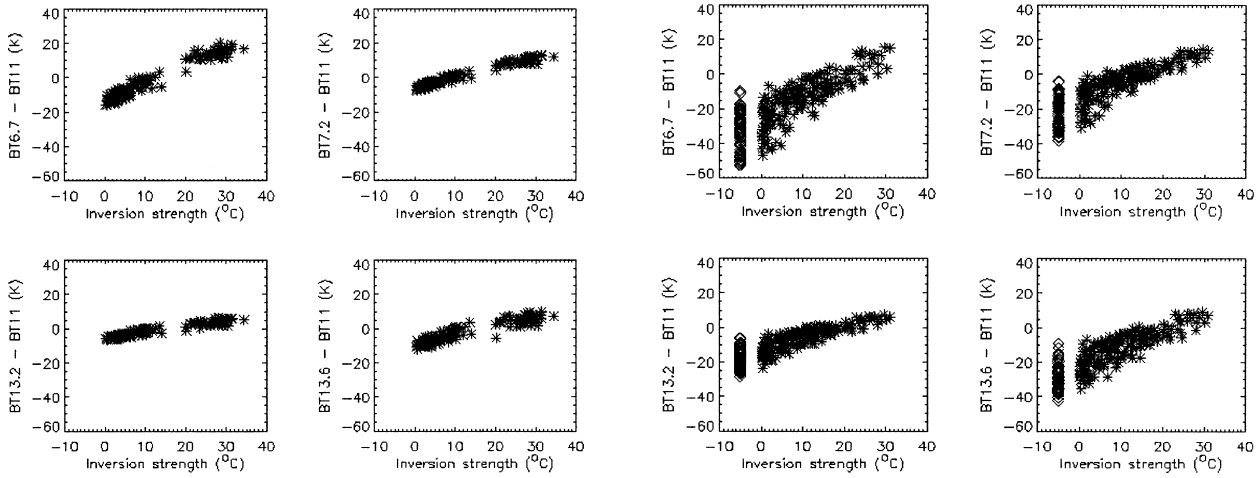

FIG. 6. Relationship between MODIS brightness temperature difference pairs and the observed temperature inversion strength over (left) high-elevation surfaces and (right) low-elevation surfaces. The diamond samples represent no inversion.

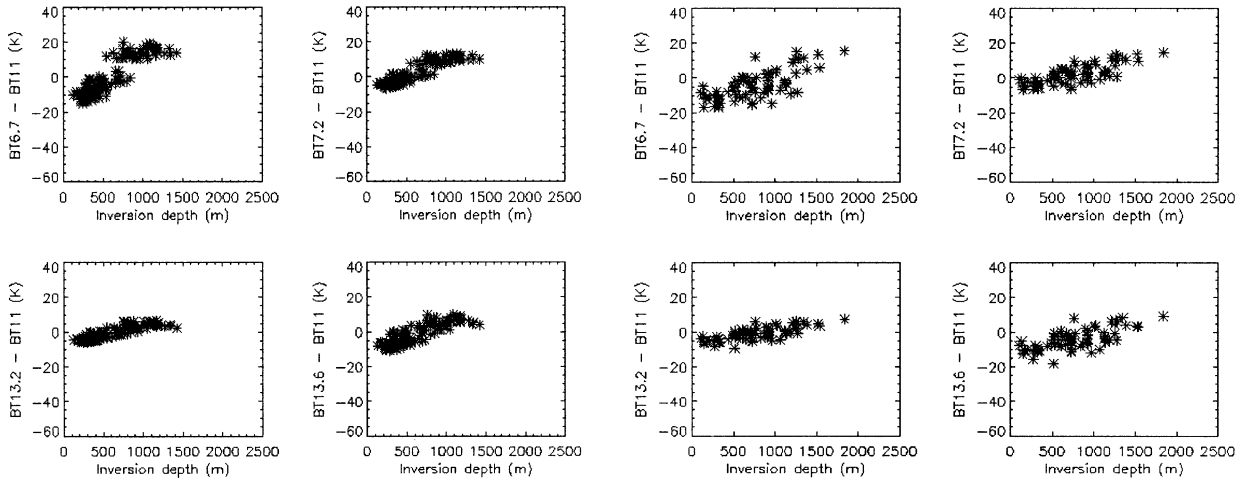

FIG. 7. Relationship between MODIS brightness temperature difference pairs and the temperature inversion depth over (left) high-elevation surfaces and (right) low-elevation surfaces.

ship between the BTDs and the temperature inversion strength is more obvious. The relationships between the observed MODIS BTDs and temperature inversion strength are shown in Fig. 8, with correlation coefficients for $BT_{6.7} - BT_{11}$, $BT_{7.2} - BT_{11}$, $BT_{13.3} - BT_{11}$, and $BT_{13.6} - BT_{11}$ of 0.80, 0.86, 0.82, and 0.78, respectively. The relationships for high-elevation surfaces are unchanged. For both high- and low-surface-elevation conditions, the relationship between temperature inversion strength and $BT_{7.2} - BT_{11}$ is stronger and less variable. Therefore, $BT_{7.2} - BT_{11}$ is used to retrieve the temperature inversion strength.

Statistical regression equations were formulated to quantify the relationship between temperature inversion strength and various combinations of MODIS infrared band brightness temperatures under both high- and low-surface-elevation conditions. For low-elevation surfaces we use

$$\Delta T = 32.2 + 0.84(BT_{7.2} - BT_{11}) - 4.63(BT_{11} - BT_{12}) - 0.081BT_{11} + 0.021(BT_{7.2} - BT_{11})^2, \quad (1)$$

where BT_{12} is the 12-μm brightness temperature (K). The 11-μm temperature is a proxy for the surface temperature, which is anticorrelated with inversion strength. The $BT_{11} - BT_{12}$ ''split window'' difference provides additional information on the column water vapor amount, which is also related to inversion strength. For high-elevation surfaces the same terms are used, with the regression yielding

$$\Delta T = 23.6 + 1.28(BT_{7.2} - BT_{11}) - 2.61(BT_{11} - BT_{12}) - 0.059BT_{11} + 0.035(BT_{7.2} - BT_{11})^2. \quad (2)$$

A total of 165 observation pairs are used to derive the coefficients of (1), with 125 observation pairs for (2). The accuracy of the retrieval is shown in Fig. 9, where the regression equations, which produce unbiased estimates, were applied to MODIS data collocated with radiosonde temperature profiles. The figures show that temperature inversion strength can be estimated with an rmse of 1.9 K for high-elevation surfaces, and an rmse of 3.2 K for low elevations. The correlation coefficients are 0.98 and 0.89, respectively (R^2 of 0.96 and 0.79). All temperature profiles are from land stations, though some are coastal, so the applicability of these equations over sea ice is not known. The retrieval error does not vary significantly with season.

To test the stability of the equations, two-thirds of the cases were randomly selected and new regression coefficients were determined. The new equations were then applied to the remaining one-third of the cases. This was repeated 1000 times. The bias of the differences between the estimated inversion strengths from (1) or (2), which are based on all cases, and from the 1000 sample regressions is 0.30 K for high surfaces and 0.20 K for low surfaces. The rms difference of the inversion strength [between (1) or (2) and the 1000 subsample regressions] is 0.38 K for high surfaces and 0.34 K for low surfaces. Results were similar with sample sizes equal to one-half the number of cases. With differences between the regressions using the full dataset and the sample regression being close to zero, the results presented in Fig. 9 would be similar if (1) and (2) were developed with an arbitrarily chosen subset of the data.

The radiosonde dataset used in this study includes 11 stations with elevations less than 250 m and 1 station with an elevation of 2800 m. What should be done for elevations between these two? When the surface elevation is higher than 2800 m, the regression equation for the high surface elevation is used. When the surface elevation is lower than 250 m, the regression equation

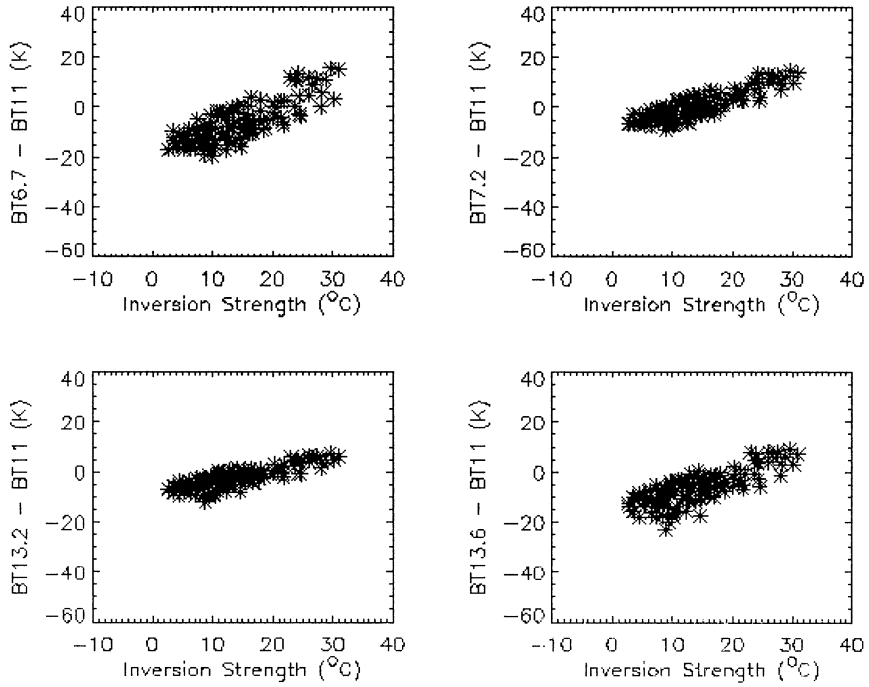

FIG. 8. Relationship between MODIS brightness temperature difference pairs and the temperature inversion strength over low-elevation surfaces after the inversion detection threshold has been applied. Compare this figure to right-hand side of Fig. 6.

for the low surface elevation is used. For locations with elevations between 250 and 2800 m, we use a linear combination of the retrieved inversion strength for high and low surfaces, weighted by the fractional distance of the actual elevation, Z, between 250 and 2800 m:

$$\Delta T(Z) = \Delta T_{\text{low}}(Z_{\text{high}} - Z)/(Z_{\text{high}} - Z_{\text{low}}) + \Delta T_{\text{high}}(Z - Z_{\text{low}})/(Z_{\text{high}} - Z_{\text{low}}) \quad (3)$$

c. Retrieval of temperature inversion depth

A similar approach can be used to estimate the inversion depth, with the relationships shown in Figs. 5 and 7. The inversion depth increases when the BTD increases or BT_{11} decreases. However, both the simulated and actual MODIS data indicate that the relationship between BTDs and temperature inversion depth is not as strong as for the inversion strength. When $BT_{6.7}$

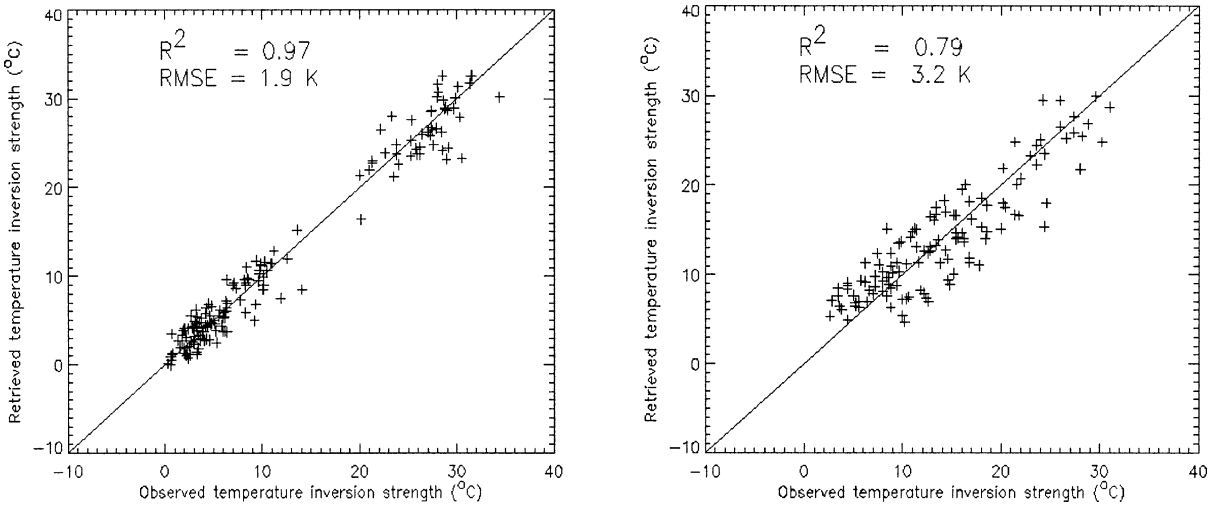

FIG. 9. Comparison of observed (radiosonde) inversion strength and retrieved (MODIS) inversion strength with (left) high-elevation surfaces and (right) low-elevation surfaces. The bias and rmse are given.

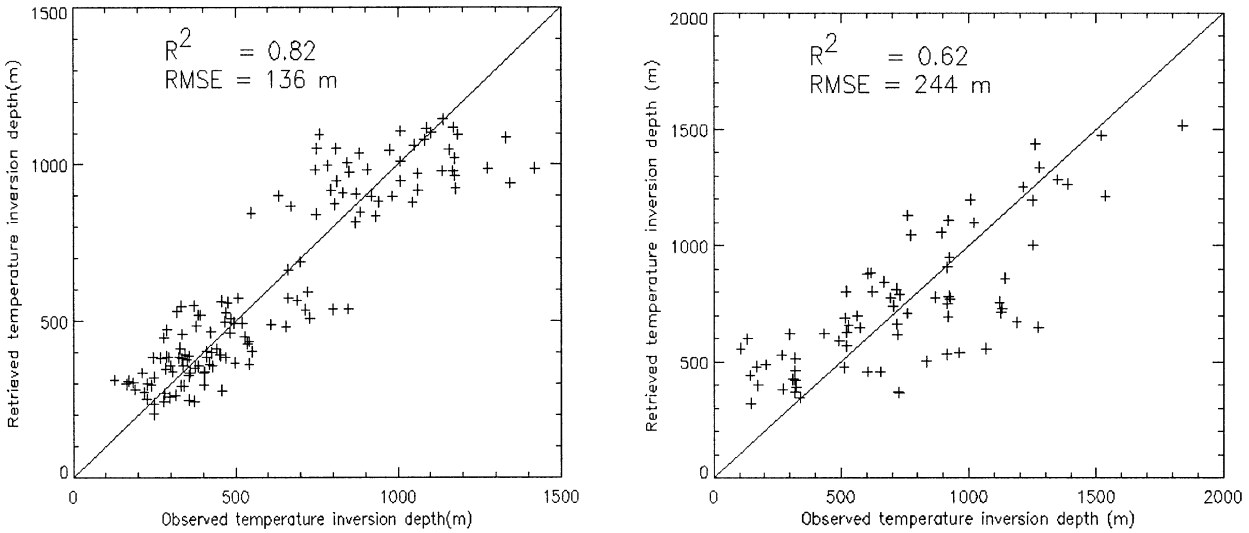

FIG. 10. Comparison of observed (radiosonde) inversion depth and retrieved (MODIS) inversion depth with (left) high-elevation surfaces and (right) low-elevation surfaces. The bias and rmse are given.

$- BT_{11}$ is larger than about 10 K, indicative of strong inversions, the relationship is weak. It was also found that when the maximum relative humidity (with respect to ice) in a profile is larger than 90%, there is no apparent linear relationship between inversion depth and BTD. So we impose a further restriction on the dataset, such that profiles with maximum relative humidities (with respect to ice) larger than 90% are excluded based on the in situ data (18% of the cases). We believe these cases to be cloudy, mislabeled in the MODIS Cloud Mask.

For low-elevation surfaces the correlation coefficients for $BT_{6.7} - BT_{11}$, $BT_{7.2} - BT_{11}$, $BT_{13.3} - BT_{11}$, and $BT_{13.6} - BT_{11}$ are 0.69, 0.73, 0.72, and 0.67, respectively. As with inversion strength, there is a somewhat stronger relationship between temperature inversion depth and $BT_{7.2} - BT_{11}$ than for the other BTD pairs. Therefore, $BT_{7.2} - BT_{11}$ is used to retrieve the temperature inversion depth. For low-elevation surfaces we use

$$\Delta Z = 720.3 + 44.1(BT_{7.2} - BT_{11}) - 133.5(BT_{11} - BT_{12}) - 0.45BT_{11} + 1.27(BT_{7.2} - BT_{11})^2. \quad (4)$$

For high-elevation surfaces the regression yields

$$\Delta Z = 1806.5 + 33.9(BT_{7.2} - BT_{11}) + 103.7(BT_{11} - BT_{12}) - 5.8BT_{11} + 0.2(BT_{7.2} - BT_{11})^2. \quad (5)$$

A total of 137 observation pairs were used to derive the coefficients in (4), with 83 observation pairs for (5). As with temperature inversion strength, if the elevation is between 250 and 2500 m, a linear combination of the retrieved inversion depth for high and low surfaces is used. A comparison of the retrieved inversion depth and the observed inversion depth is shown in Fig. 10. The figures show that temperature inversion depth can be estimated with an rmse of 137 m for high-elevation surfaces, and an rmse of 244 m for low elevations. The correlation coefficients are 0.91 and 0.79, respectively.

d. Error sources

Errors in the retrievals of inversion strength and depth may originate from a variety of sources. First, radiosonde data for the lower-elevation stations is of relatively low vertical resolution. Both the inversion strength and depth used as truth may be inaccurate as a result. These errors can be as high as 0.5 K and 88 m, respectively.

Second, inversion structure can differ significantly from the more ideal shape shown in Fig. 2. For example, the two profiles in Fig. 11 have similar inversion strengths (18.4 and 20.2 K) and depth (1203 and 1272 m). For profile A $BT_{7.2} - BT_{11}$ is 1.0 K but for profile B is 5.0 K. With the same temperature inversion strength and depth, the BTDs will be different if the total water vapor amount or its vertical distribution is different, as this affects the shape of the weighting function of each channel. The BTDs can therefore exhibit a broad range of values for the same temperature inversion strength and depth, as shown in Figs. 6 and 7. This enters into the regression as greater variability in the data points and a lower statistical significance of the regression coefficients.

Third, there is some uncertainty in the MODIS Cloud Mask product, which we use to identify clear-sky pixels. The detection of low- and midlevel clouds at night is most problematic. Cloudy pixels will have small, neg-

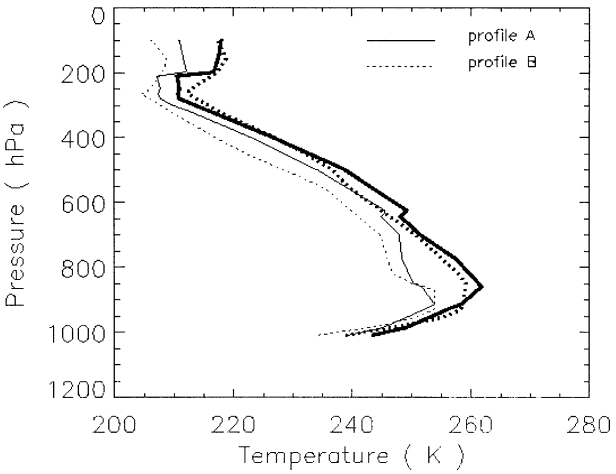

FIG. 11. Radiosonde temperature (thick lines) and dewpoint temperature (thin lines) profiles from station 24266 on 22 Oct (solid) and 25 Oct (dotted) 2001.

ative BTDs but generally weaker inversions than clear pixels. Therefore, false clear pixels in the data used for the regression analyses could result in coefficients that underestimate inversion strength and height for weaker inversions but overestimate them for stronger inversions. However, given the agreement between simulated and observed BTDs (Figs. 4 and 5 compared to Figs. 6 and 7), cloud contamination does not appear to have significantly affected the results. A visual inspection of the cloud mask for many of the images used in the analyses supports this conclusion.

5. Application and comparison to other datasets

An application of the methods presented above is shown in Fig. 12 for inversion strength and in Fig. 13 for inversion depth over the Arctic and Antarctic for a single winter day. The images are composites of consecutive MOD07_L2 overpasses, subsampled to 10-km resolution. No results are given for cloudy areas (white). For the Arctic, inversion strength varies from 0° to 30°C. In the coastal areas and the northern portions of the Greenland and Norwegian Seas, the inversion strength is weak because of turbulent mixing over the open water. Inversion strength over the pack ice is stronger, with values in the range 12°–18°C. Inversion strength generally increases inland due to stronger surface radiative cooling.

The spatial pattern of inversion depth is similar to that of inversion strength. It ranges from 0 to 1500 m over the Arctic, with a minimum at some coastal areas and near the ice edge. The greatest inversion depth and strength are found near the Yenisey River valley, the Lena River valley, and the Kolyma River valley in Russia and Siberia, where the cold air drainage associated with the strong wintertime Siberian high pressure cell results in strong temperature inversions (Serreze et al. 1992). Over Greenland, the inversion strength and inversion depth are moderately large due to the strong surface radiative cooling.

The inversion strength over the Antarctic Plateau is greater than that in the Arctic, primarily due to the stronger high surface radiative cooling. Inversion strength and depth increase with increasing surface elevation. The maximum inversion strength is near 40°C, and maximum inversion depth is approximately 1500 m.

Temperature inversion strength and inversion depth can also be derived from the NCEP profile data. The NCEP inversion strengths for both clear and cloudy conditions are shown in Fig. 14, corresponding in time and space to the clear-sky MODIS retrievals in Figs. 12 and 13. The NCEP data are presented only to illustrate the general patterns in inversion characteristics. The inversion strength has a similar spatial distribution for both

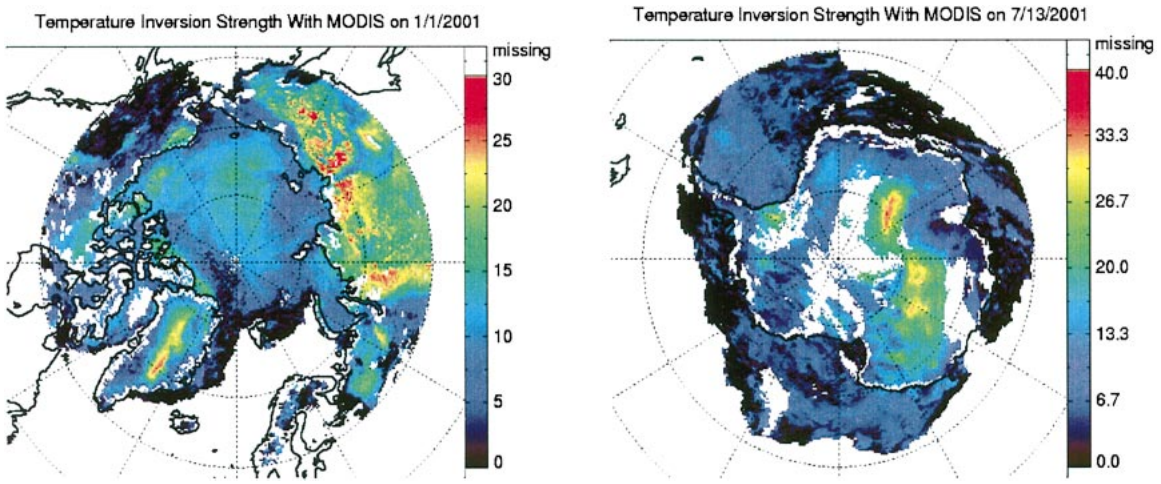

FIG. 12. Temperature inversion strength (°C) estimated from MODIS over the (left) Arctic and (right) Antarctic on a single winter day for each hemisphere.

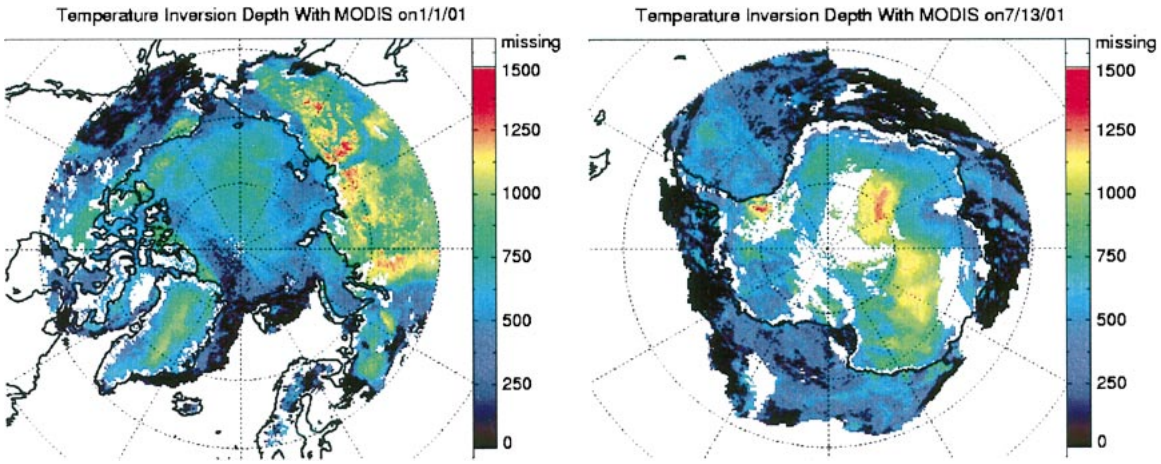

FIG. 13. Temperature inversion depth (m) estimated from MODIS over the (left) Arctic and (right) Antarctic on a single winter day for each hemisphere.

polar regions, with large inversion strengths over land and the interior pack ice and smaller values over coastal areas. However, the MODIS image provides more spatial detail and accurate results, based on comparisons with radiosonde data. Overall, inversion strengths from MODIS are larger than those from NCEP. This is due in part to the low vertical and horizontal resolutions of the NCEP data, where there are only seven pressure levels lower than 400 hPa in the NCEP data and the horizontal resolution is 2.5° latitude × 2.5° longitude. A comparison with inversion depth from the NCEP data produced similar results.

The MODIS regression retrievals were compared to inversion characteristics derived from the MOD07_L2 temperature profile product. The MOD07_L2 product uses a physical (as opposed to statistical) retrieval method to get the temperature profile at 20 pressure levels. It is also for clear skies only. The 20 pressure levels are 5, 10, 20, 30, 50, 70, 100, 150, 200, 250, 300, 400, 500, 620, 700, 780, 850, 920, 950, and 1000 hPa. Inversion strength from the MODIS regression retrievals, the MOD07_L2 temperature profile product, and radiosonde data are shown in Fig. 15. The inversion strengths from the MOD07_L2 product are biased low, and both the bias and standard deviation increase for stronger inversions. This in turn produces a large rmse when compared to radiosonde data. As with the NCEP data, this is in part due to the relatively low vertical resolution.

6. Conclusions

A method for estimating the strength of low-level atmospheric temperature inversions using clear-sky infrared data from the MODIS instrument has been presented. The method involves an empirical relationship between the inversion strength, defined as the temperature difference across the inversion, or depth, defined

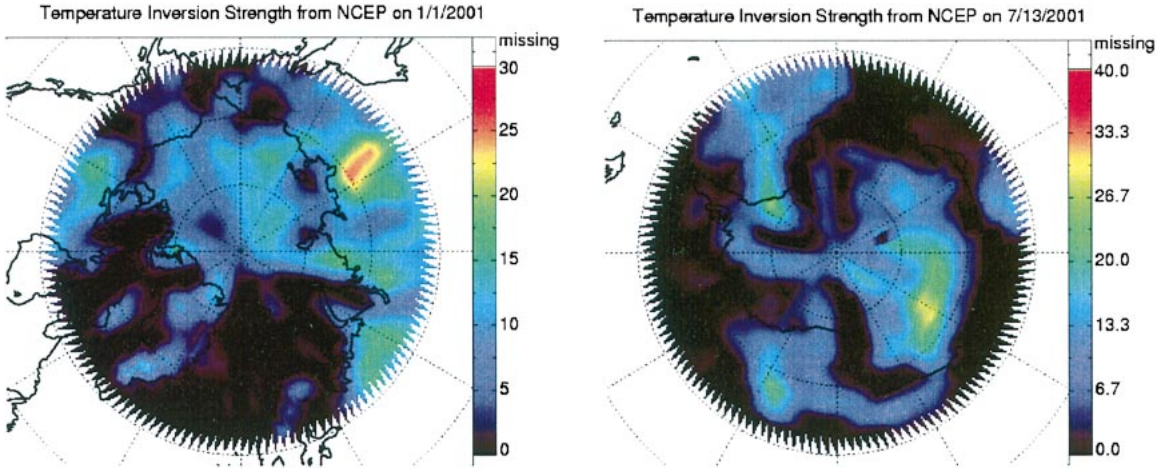

FIG. 14. Temperature inversion strength (°C) estimated from the NCEP reanalysis over the (left) Arctic and (right) Antarctic on a single winter day for each hemisphere (the same days as shown in Figs. 12 and 13).

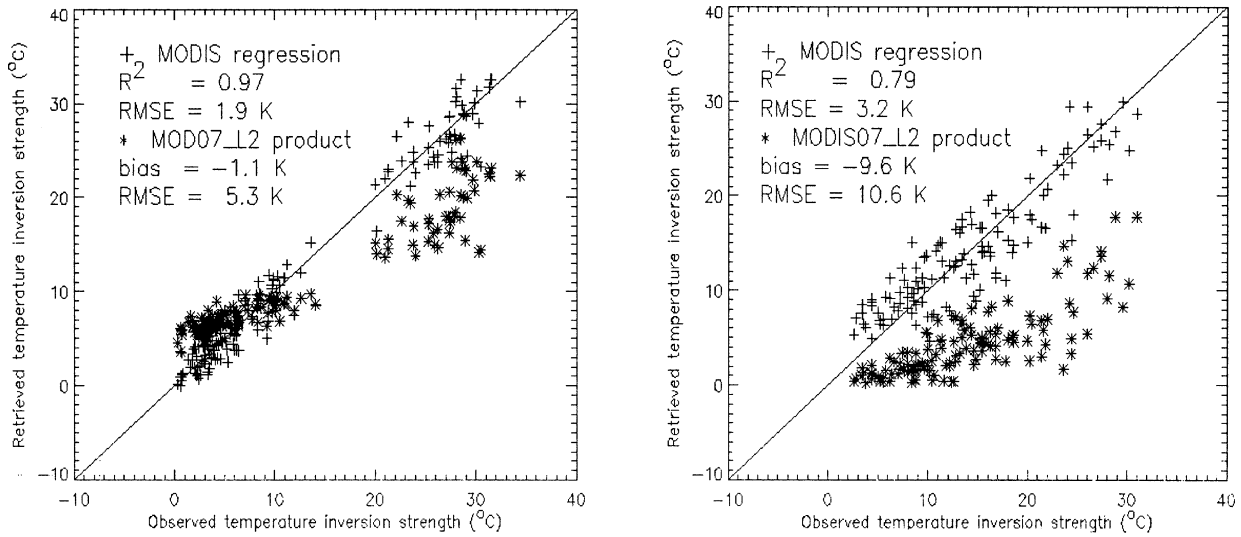

FIG. 15. Inversion strength from the MODIS regression retrievals and from the MOD07_L2 product compared to radiosonde observations for (left) high surface elevations and (right) low surface elevations.

as the altitude difference, and the difference between satellite-measured brightness temperatures in the 7.2-μm water vapor and 11-μm infrared window bands. Results from all seasons indicate that inversion strength can be estimated unbiasedly with a root-mean-square error (rmse) of 2°–3°C. The method is more accurate for high-elevation surfaces (1.9 K rmse, $R^2 = 0.97$), characterized by stronger inversions, than for low-elevation surfaces (3.2 K rmse, $R^2 = 0.79$). Inversion depth can be estimated with an rmse of 130–250 m ($R^2 = 0.82$ and 0.62).

The method is only for clear-sky conditions. Inversions under clouds are generally weaker (lower temperature difference) and shallower (lesser depth). The fact that Arctic and Antarctic cloud amounts are large—in the range of 60%–80% depending on the location—means that clear-sky inversion retrievals represent, on average, less than half of the area. This must be considered if retrievals are used in climatological studies, and when clear-sky inversions from MODIS are compared to other inversion datasets.

Satellite retrievals of inversion strength and inversion depth can be used to validate, and potentially improve, the parameterization of energy transfer processes in climate models. Parameters based on the estimated inversion strength, inversion depth, and the bulk boundary layer wind shear may be useful for monitoring climate change. With MODIS, temperature inversions can be observed at a spatial resolution as high as 1 km^2 and a temporal sampling of up to 14 times per day, providing an opportunity for detailed studies of the spatial distribution and temporal evolution of the high-latitude boundary layer.

Acknowledgments. This work was supported by NASA Contract NAS5-31367 and by the NOAA Product Systems Development and Implementation program. Thanks are due to Mat Gunshor for generating the weighting function data.

REFERENCES

Ackerman, S. A., 1996: Global satellite observations of negative brightness temperature differences between 11 and 6.7 μm. *J. Atmos. Sci.*, **53,** 2803–2812.

Bradley, R. S., F. T. Keiming, and H. F. Diaz, 1992: Climatology of surface-based inversions in the North American Arctic. *J. Geophys. Res.*, **97,** 15 699–15 712.

——, ——, and ——, 1993: Recent changes in the North American Arctic boundary layer in winter. *J. Geophys. Res.*, **98,** 8851–8858.

Kahl, J. D., 1990: Characteristics of the low-level temperature inversion along the Alaskan Arctic coast. *Int. J. Climatol.*, **10,** 537–548.

Key, J., and A. J. Schweiger, 1998: Tools for atmospheric radiative transfer: Streamer and FluxNet. *Comput. Geosci.*, **24,** 443–451.

King, M. D., and Coauthors, 2003: Cloud and aerosol properties, precipitable water, and profiles of temperature and water vapor from MODIS. *IEEE Trans. Geosci. Remote Sens.*, **41,** 442–458.

Mahesh, A., V. P. Walden, and S. G. Warren, 1997: Radiosonde temperature measurements in strong inversions: Correction for thermal lag based on an experiment at the South Pole. *J. Atmos. Oceanic Technol.*, **14,** 45–53.

Serreze, M. C., J. D. Kahl, and R. C. Schnell, 1992: Low-level temperature inversions of the Eurasian Arctic and comparisons with Soviet drifting stations. *J. Climate*, **5,** 615–630.

Stone, R. S., and J. D. Kahl, 1991: Variations in boundary layer properties associated with clouds and transient weather disturbances at the South Pole during winter. *J. Geophys. Res.*, **96,** 5137–5144.

Walden, V. P., A. Mahesh, and S. G. Warren, 1996: Comment on ''Recent changes in the North American Arctic boundary layer in winter'' by R. S. Bradley et al. *J. Geophys. Res.*, **101,** 7127–7134.